

Mass reconstruction with M_2 under constraint in semi-invisible production at a hadron collider

Partha Konar^{1,*} and Abhaya Kumar Swain^{1,†}

¹*Physical Research Laboratory, Ahmedabad-380009, India*

Abstract

The mass-constraining variable M_2 , a $(1+3)$ -dimensional natural successor of extremely popular M_{T2} , possesses an array of rich features having the ability to use on-shell mass constraints in semi-invisible production at a hadron collider. In this work, we investigate the consequence of applying a heavy resonance mass-shell constraint in the context of a semi-invisible antler decay topology produced at the LHC. Our proposed variable, under additional constraint, develops a new kink solution at the true masses. This enables one to determine the invisible particle mass simultaneously with the parent particle mass from these events. We analyze in a way to measure this kink optimally, exploring the origin and the properties of such interesting characteristics. We also study the event reconstruction capability inferred from this new variable and find that the resulting momenta are unique and well correlated with true invisible particle momenta.

PACS numbers: 12.60.-i, 14.80.Ly, 11.80.Cr

Keywords: Beyond Standard Model, Hadronic Colliders, Particle and resonance production

*Electronic address: konar@prl.res.in

†Electronic address: abhaya@prl.res.in

I. INTRODUCTION

The Large Hadron Collider (LHC), after the successful completion of its first run and the remarkable achievement of the Higgs boson discovery [1, 2], has already entered into its second phase. Upgraded with higher energy and luminosity, the main physics goal is to explore the multi-TeV scale associated with the physics beyond the Standard Model (BSM). Although the LHC has not reported any clinching evidence for new physics so far, expectations are running high for possible new physics signals in soon unless such signatures are already hidden inside the LHC data. Any scenario with a positive outcome essentially demands the measurements of the mass, coupling and spin of new BSM particles. However, this is going to be complex since many of the very likely scenarios with a wide class of BSM models have embraced the concept of thermal relic dark matter (DM) as some stable exotic member within them. Since these massive DM particles are colorless, electrically neutral and weakly interacting, once produced in the collider, they do not leave any trace at the detector. Hence, one needs to rely on the experimentally challenging signature of missing transverse momenta \vec{P}_T from the imbalance of total transverse momentum, accounting for all visible decay products in each event from an already adverse jetty environment of the hadron collider. Moreover, the DM in many models is expected to produce in pairs because of its stabilizing symmetry,¹ commonly associated with the Z_2 parity, which makes the event reconstruction even more challenging.

Keeping an eye on the above encumbrances, many ideas have already been developed for the determination of mass and spin. For some recent reviews, see Refs. [8, 9] for different mass measurement techniques. To give a brief and sketchy classification for the mass measurement techniques, parts of which are also crucial for our study, one looks into the following:(a) In the end-point method [10–16], the end point of the independently possible invariant mass constructed out of all combinations of visible particles is related to the unknown masses involved in a decay chain. Thus, a sufficient number of end-point measurements are needed to pin down all the unknown masses, which is only possible for a longer decay chain. (b) The polynomial method [17–21] tries to solve for all unknowns (unknown masses

¹ There can be a DM stabilizing symmetry other than Z_2 which allows more than one DM particle per vertex and kinematic variables [3–7] were used to distinguish between the DM stabilizing symmetries, but we stick to the popular Z_2 parity for simplicity and extendability.

and invisible particle four momenta) in the event, using all available constraints. Again all unknown masses can be determined only if one has at least a three-step decay chain.

(c) The transverse mass methods are based on transverse mass variables defined by the minimum parent mass consistent with minimal kinematic constraints in the event, for a given trial mass of the invisible particle. Here constraints consist of the equality of parent mass, mass-shell relations and the missing transverse momenta from undetected invisible particles. Several interesting features of these variables received lots of attention recently. The transverse mass variables were further extended with many variants, such as, M_{T2} [22–30], subsystem M_{T2} [31], $M_{T2\perp}$ and its sister $M_{T2\parallel}$ [32], M_{CT2} [33, 34], asymmetric M_{T2} [35, 36], contranverse mass M_{CT} [37–39], $M_{CT\perp}$ and its sister $M_{CT\parallel}$ [40]. In Ref. [41, 42] it is shown that the $(1 + 3)$ -dimensional generalization of M_{T2} can be useful, where one can apply the equality of parent mass and/or equality of relative² mass constraints to improve the number of events at the end point. (d) Inclusive variables are the ones whose construction do not take into account the production mechanism or topology of the new particles and only depend on the final state visible particles momenta and missing transverse momenta in the event. There are many inclusive variables, such as H_T [43], total visible invariant mass M [44], \cancel{E}_T , effective mass M_{eff} [10], \hat{s}_{min} and its sisters [45–48]. They are useful for extracting the mass scale of new physics in a model independent way. While each method is more relevant for a particular outlook, the transverse mass variable and its extensions turned out to have the potential for precise measurement of the masses in short single-step decay chains involving invisible particles. Consequently, for our present analysis, we further develop and discuss this method in the next section.

The present work is inspired from another class of prescriptions known as the cusp method [49–52], which can determine both the parent and invisible particle (or DM) masses simultaneously from single-step decay chains. However, the primary assumption is that both the parents are produced from an on-shell heavy resonance, whose mass is known already. This method uses the measured momenta of visible particles and constructs possible variables, among which the invariant mass and magnitude of the individual transverse momenta of the visible particle can exhibit non-smooth structure or cusp and end point in their distributions. The location of this cusp and end point are function of the unknown masses, so the

² Relative is defined by any resonance other than parent and daughter realised in some particular topology.

parent and daughter mass can be determined simultaneously from these two measurements. It is argued that the longitudinal boost invariant variables, such as the individual transverse momenta and the invariant mass of visible particles, are minimally affected by the unknown transverse boost, which are sufficient to pin down both the unknown masses. This analysis was extended further in the context of the linear collider ($\ell^+\ell^-$) [52].

In this paper, we propose a complementary procedure to measure both the parent mass and daughter mass simultaneously using the M_2 variable. We also assume that the heavy resonance mass is known, and this information is embedded in the minimization of M_2 resulting in a new constrained variable dubbed M_{2Cons} . Further discussion on this variable is in Sec. II with formal definitions and chronological motivations. Emboldened by the interesting characteristic of this variable which develops a kink in the distribution end-point maxima corresponding to the correct value of the unknown invisible mass, we propose a simultaneous measurement of both the masses by identifying the kink position. We also put forward a desirable way of recasting the kink by utilizing all available data, giving a robust outcome irrespective of other realistic effects. This M_{2Cons} variable proved to be useful in all mass range, including the region known as the ‘large mass gap’ in the kinematic cusp method where the cusp may not be very sharp. A unique event reconstruction can also be realized using M_{2Cons} .

As a (1+3)-dimensional variable, M_2 has the capability to use all components of three momenta. Thus, the utilization of additional mass constraints is possible if such information is available. This brings additional advantages, contrary to the transverse mass variables, which by construction are not similarly capable. Here we argue that the newly developed M_{2Cons} variable equips one to consider additional constraint from on-shell mass resonance, which in turn produces suitable kinematic constraints to get a new kink solution in antler topology. Importantly, this contribution towards the kink is not merely symbolic but is substantive, enabling better mass measurements.

This paper is organized as follows. In Sec. II, we motivate the antler production topology at the hadron collider describing all available constraints associated with such topology. In this context, we also open up discussion on the M_{T2} transverse mass variable and its (1+3)-dimensional generalized sisters in the M_2 family. Following that, we introduce our new variable M_{2Cons} . We further discuss the effect of an additional heavy resonance constraint, describing the basic features and benefits of this variable. Sec. III is assigned to describing

the kink solution coming from the M_{2Cons} distribution end point as a function of the trial invisible mass which is yet unknown. Further comparison is made with the corresponding maximum achievable in the M_2 variable. Realizing that the number of events at the end point is very limited for M_{2Cons} , we formulated an efficient way in Sec. IV to reconstruct the kink by recasting all available data. In Sec. V, we show that M_{2Cons} can be used for a unique event reconstruction, and the reconstructed momenta are well correlated with the true momenta of the invisible particle. Finally, in Sec. VI we summarize our main results and conclude.

II. ANTLER TOPOLOGY AND CONSTRAINED VARIABLE WITH M_2

Antler topology, realized in different Standard Model (SM) processes and a variety of new physics models, is very common and widely explored. The SM Higgs boson decaying semi-invisibly through the W-boson,³ $h \rightarrow W + W^* \rightarrow \ell\nu + \ell\nu$, or via τ lepton, $h \rightarrow \tau + \tau \rightarrow W^*\nu_\tau + W^*\nu_\tau$, are some of the significant channels in the context of the SM Higgs search at the LHC. Similarly, in several BSM theories, the search strategy relies on antler production topology. Some of these include the heavy Higgs of supersymmetry (SUSY) decaying to the Z-boson and lightest supersymmetric particle (LSP) via neutralinos, $H \rightarrow \tilde{\chi}_2^0 + \tilde{\chi}_2^0 \rightarrow Z\tilde{\chi}_1^0 + Z\tilde{\chi}_1^0$ [53] and the SUSY extended Z' decaying to the lepton and LSP via the slepton, $Z' \rightarrow \tilde{\ell}^+ + \tilde{\ell}^- \rightarrow \ell^+\tilde{\chi}_1^0 + \ell^-\tilde{\chi}_1^0$ [54, 55]. Similarly, in a universal extra-dimensional model, second excitation states can decay to first excitation states, $Z^{(2)} \rightarrow L^{(1)} + L^{(1)} \rightarrow \ell^-\gamma^{(1)} + \ell^+\gamma^{(1)}$ [56, 57]. The semi-invisible decay of doubly charged exotic scalars in many BSM scenarios can produce SM particles via W pairs, $\phi^{++} \rightarrow W^+ + W^+ \rightarrow \ell^+\nu_\ell + \ell^+\nu_\ell$ [58]. Moreover, the heavy Higgs or heavy Z' can also decay semi-invisibly to SM particles via $t\bar{t}$ pairs, $H/Z' \rightarrow t + \bar{t} \rightarrow bW^+ + \bar{b}W^- \rightarrow b\ell^+\nu_\ell + \bar{b}\ell^-\nu_\ell$. In addition, antler topology can also be realized at the linear collider as fixed c.m. energy is equivalent to the heavy resonance produced at its rest frame before pair production and subsequent decay (for example, see [52]).

Before starting our analysis, let us describe the basic setup and the notation. The rep-

³ Note that except from the fact that $h \rightarrow W + W^*$ probably signify most familiar SM antler channel, this off-shell production of W is not pursued further in present analysis.

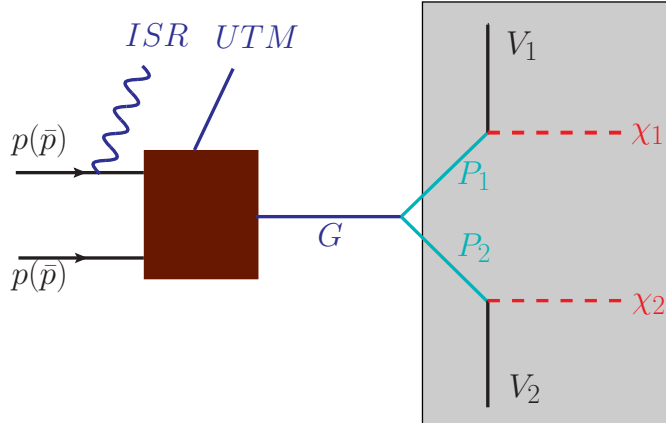


FIG. 1: Archetype of antler topology where G , a heavy resonance particle with mass m_G produced at hadron collider, decays to two daughter particles P_1 and P_2 through two-body decay, each of which subsequently decays to produce SM visible particle (V_i) and an invisible or dark matter particle (χ_i). Momenta of these visible and invisible particles are assigned as p_i and q_i , respectively. m_P and m_χ are masses of parent P_i and invisible particle χ_i . This topology can be considered for SM Higgs production with subsequent decays into SM visible and massless neutrinos as invisible particles. On the other hand, in a BSM scenario, G (a parity-even state) can decay to produce (parity-odd states) P_i and χ_i .

representative diagram for antler topology is shown in Fig. 1, where a parity-even⁴ heavy resonance particle G (grandparent) with mass m_G decays to two parity-odd particles P_1 and P_2 , each of which subsequently decays to the Standard Model particle (V_i) and an invisible or dark matter particle (χ_i). We assign the momenta to visible and DM particles in each side of the decay chain as p_i and q_i , respectively. Moreover, we denote the masses of parents (P_i) and invisible daughters (χ_i) as m_P and m_χ , respectively. The primary motivation of this analysis is to determine these unknown parameters. Though we have shown a generic antler topology in Fig. 1, in this analysis we are interested in the symmetric antler process motivated by the above examples. The symmetric antler includes same parent ($P_1 = P_2$) and same daughter ($\chi_1 = \chi_2$) particles, or at least their masses are same, $m_{P_1} = m_{P_2} = m_P$ and $m_{\chi_1} = m_{\chi_2} = m_\chi$.

We would like to address this topology using the mass-constraining variable for the sub-

⁴ Parity is pertinent only for the BSM processes having stable invisible exotic particles in the final state.

system represented by the gray shaded region shown in Fig. 1. Let us start with the existing and popular transverse mass variable M_{T2} before moving into the generalization and finally extending to our new variable. M_{T2} is defined to have the potential to measure the masses of the BSM particles both in short or long decay chains, although its dominance and significance is mostly grounded in its capability to handle the former case. The classic definition⁵ of M_{T2} is given by the larger value between two transverse masses $M_T^{(i)}$ constructed from both sides of the decay chain and minimized over unknown invisible momenta satisfying the \vec{P}_T constraints of that event. Mathematically,

$$M_{T2} \equiv \min_{\substack{\vec{q}_{iT} \\ \{\sum \vec{q}_{iT} = \vec{P}_T\}}} \left[\max_{i=1,2} \{M_T^{(i)}(p_{iT}, q_{iT}, m_{vis(i)}; m_\chi)\} \right] \quad (1)$$

with the usual definition of the transverse mass for each decay chain,

$$\begin{aligned} (M_T^{(i)})^2 &= m_{vis(i)}^2 + m_\chi^2 + 2(E_T^{vis(i)} E_T^{inv(i)} - \vec{p}_{iT} \cdot \vec{q}_{iT}) \\ E_T^{vis(i)} &= \sqrt{m_{vis(i)}^2 + p_{iT}^2}, \quad E_T^{inv(i)} = \sqrt{m_\chi^2 + q_{iT}^2}. \end{aligned} \quad (2)$$

$(E_T^{vis(i)}, \vec{p}_{iT})$ and $(E_T^{inv(i)}, \vec{q}_{iT})$ are (1+2)-dimensional transverse energy-momenta corresponding to the visible and the invisible decay products in the i^{th} decay chain, respectively. Note that, in the definition of M_{T2} , the minimization is done over all possible partitions of \vec{P}_T and the maximization of $M_T^{(i)}$ within the bracket ensures a closer shot towards the parent mass m_P . By this definition, M_{T2} , calculated for each event, must be smaller than or equal to m_P .

The maximum quantity for any of these mass variables $M_{...}$ (such as, M_{T2} , M_2 or M_{2Cons}) over the available data set is

$$M_{...}^{max}(m_\chi) \equiv \max_{\{All\ events\}} [M_{...}(m_\chi)]. \quad (4)$$

Now M_{T2}^{max} should provide a very close estimate of m_P . Moreover, in the scenario where the invisible particle mass is a priori unknown, *e.g.* dark matter models, $M_{T2}^{max}(\tilde{m}_\chi)$ would still offer a useful correlation with the trial invisible mass \tilde{m}_χ , a daughter mass hypothesis

⁵ Here, “ T ” and “ 2 ” in M_{T2} stands for the *transverse projection* and *two parent particles*, respectively, in the topology under examination. Reference [9] generalized and unified the concept of mass variables and set a preferred nomenclature according to the order of operations to rewrite the same variable as M_{2T} within a general M_2 family. Notably, [9] also demonstrated the fact that the transverse projection can be done using not one, but three completely different schemes.

used as an input for the calculation of M_{T2} . One can possess only this partial information on the unknown parent and daughter masses unless, under *some special circumstances*, this correlation curve generates a kink feature exactly at the correct mass point. We will have a slightly elaborate discussion about the kink feature in Sec. III.

Now to motivate the (1+3)-dimensional generalization of previous definitions as in Eq. 1, one readily notes that the M_{T2} is not utilizing longitudinal components of the momenta and, thus, the available mass-shell constraints for a given topology. M_2 is thus constructed [9] out of the (1+3)-dimensional momenta by removing all “ T ” in the definition of Eqs. 1-3 (except that of the total missing transverse momentum constraint under the curly bracket, since the longitudinal part is not available in the context of the hadron collider). Now one can apply the on-shell mass constraints in the minimization of M_2 , and, depending on the constraints applied, different constrained classes of the M_2 variable (*e.g.* M_{2xx} , M_{2cx} and M_{2cc}) can be constructed; details about these variables can be found in Ref. [42]. Using similar notation, one can readily come up with the first two types of variables available from the subsystem considered in Fig. 1. Here, M_{2cx} is the (1+3)-dimensional generalization of M_{T2} with the equality of the parent mass constraint applied in the minimization,

$$M_{2cx} \equiv \min_{\vec{q}_1, \vec{q}_2} \left[\max_{i=1,2} \{M^{(i)}(p_i, q_i, m_{vis(i)}; m_\chi)\} \right]_{\left\{ \begin{array}{l} \vec{q}_{1T} + \vec{q}_{2T} = \vec{p}_T \\ (p_1 + q_1)^2 = (p_2 + q_2)^2 \end{array} \right\}} \quad (5)$$

with the (1+3)-dimensional mass from each decay chain as

$$(M^{(i)})^2 = m_{vis(i)}^2 + m_\chi^2 + 2(E^{vis(i)} E^{inv(i)} - \vec{p}_i \cdot \vec{q}_i). \quad (6)$$

The corresponding M_{2xx} variable is simply perceived once the last constraint inside bracket is absent, just like the transverse mass case in Eq. 1. It is straightforward to show [42]

$$M_{T2} = M_{2xx} \equiv M_2 \quad (7)$$

$$= M_{2cx}. \quad (8)$$

Also note that, in our example, there is one visible particle per decay chain in the final state. Hence, the M_{T2} and other variables always come from a balanced configuration irrespective of the choice of trial invisible mass. So once again the maximum M_{T2}^{max} (or the maxima of other variables as in Eq. 7 and Eq. 8) can only give a constraint between parent and invisible particle mass.

Now, by following the steps before the subsystem as in Fig. 1, one realizes that the parents (P_1, P_2) are actually originated from a heavy resonance (G). In a BSM scenario, even-parity G can directly decay to SM observable particles and hence the mass, m_G , can in principle be measured. Here, before we move further, we assume that in our topology only this heavy resonance mass m_G is known. We are now in a position to develop a variable using this mass constraint, so that⁶

$$M_{2Cons}(\tilde{m}_\chi) \equiv \min_{\vec{q}_1, \vec{q}_2} \left[\max_{i=1,2} \{M^{(i)}(p_i, q_i, m_{vis(i)}; \tilde{m}_\chi)\} \right], \quad (9)$$

$$\left\{ \begin{array}{l} \vec{q}_{1T} + \vec{q}_{2T} = \vec{q}_T \\ (p_1 + p_2 + q_1 + q_2)^2 = m_G^2 \end{array} \right\}$$

where $(1+3)$ -dimensional invariant mass is $M^{(i)}$ as in Eq. 6. Additionally, the dependence on the unknown trial invisible mass \tilde{m}_χ is shown explicitly. With this additional constraint, one expects a squeezed phase space affecting this new variable from that of M_2 ; furthermore, we will soon realize that this effect is a little more far-reaching. Before we gradually move to demonstrate that, let us open the discussion with the consequences of this new variable in the invisible momenta space.

The additional heavy resonance mass-shell constraint in the minimization (last condition inside bracket of Eq. 9) constrains the invisible particle momenta, such that, the invariant mass of the parents is confined to a narrow resonance of mass m_G . This phenomenon is true for each event. In Fig. 2, the effect of this constraint is demonstrated for one event with an example where the trial invisible particle mass \tilde{m}_χ is considered smaller than the yet unknown true mass m_χ . The region represented by the light temperature map color gradient is the maximum between two transverse masses $M_T^{(i)}$, as in Eq. 1 before executing the minimization. This is shown with respect to the invisible momenta components, q_{1x} and q_{1y} , by taking care of the missing transverse momenta constraints. Now the minimum of this quantity, which is nothing but the M_{T2} , is the minimum point in the color map displayed by the filled circle \bullet , and different contour lines are shown by *dashed curves*. Moving to our $(1+3)$ -dimensional new variable with the heavy resonance mass-shell constraint in Eq. 9, once again after doing the similar exercise we get the *solid contour curves* superimposed in the same plot. Of course, we are no longer showing the color gradient as done in the transverse

⁶ One can also consider an additional constraint using the equality of parent mass $(p_1 + q_1)^2 = (p_2 + q_2)^2$ in M_{2Cons} . Although this would further constrain the allowed invisible momentum space, it would finally choose the same minima. Hence, our arguments with this present example and analysis remain the same.

mass case. Transformation of dashed contour lines into corresponding solid ones (same color represents the same value of that contours) within the same region qualitatively indicate the effect of this additional mass constraint. Minimum of these solid contours represents the M_{2Cons} , displayed by circle plus \oplus in the same figure. Note that the longitudinal momenta components for the invisible pairs are eliminated in this demonstration by minimizing with the G mass-shell constraint.

As noted, m_G constraint restricts the invisible momenta making the region shrink as depicted by the dashed and solid contour (*e.g.* following blue lines correspond to 100 GeV), the dashed line contour does not satisfy the additional G mass-shell constraint while solid contour does. The same is true for all other lines also. The represented values of M_{T2} and M_{2Cons} considered in this example are 75.1 and 98.5 GeV, respectively, for trial mass \tilde{m}_χ at 10 GeV which is smaller than the true invisible mass 100 GeV. The corresponding true mass of parents and heavy resonance are 200.0 and 1000.0 GeV, respectively. The white dashed (solid) line represents the equality of the transverse-mass (mass) of parents and this equality line has moved towards higher value because of the constraint. As a result, one naturally expects $M_{2Cons} \geq M_2$ event by event. The red star \star is the position of the true transverse momenta of the invisible particle. Clearly, constraint brings the minima, M_{2Cons} , closer to the true momenta, and this can improve any effort to reconstruct the invisible momenta. This feature will be further considered and discussed in Sec. V.

One more remarkable feature emerges at this point which will be capitalized in the next section. We already noted the event wise upward shift of values under the constraint. The next natural question in this context concerns the maximum value achievable by this mass variable and how it is related to the trial missing particle mass? The experimentally measured maxima can deviate (downward) from the theoretical maximum of the mass variable depending upon the accessible number of events, and more importantly, the abundance of events towards the end point of the distribution. We postpone this issue for the time being and consider it again in Sec. IV. Now coming back to our variable, it should not be surprising that at the true value of the invisible particle mass (*i.e.* when $\tilde{m}_\chi = m_\chi$), the maximum value of the constraint variable M_{2Cons}^{max} coincides with that of the variable without this constraint, M_2^{max} . This is because both of these variables are derived for the same topology. On the other hand, at all other trial mass values, not only is the individual (event-by-event) constraint quantity larger, but also the maximum of that constraint mass is the larger value.

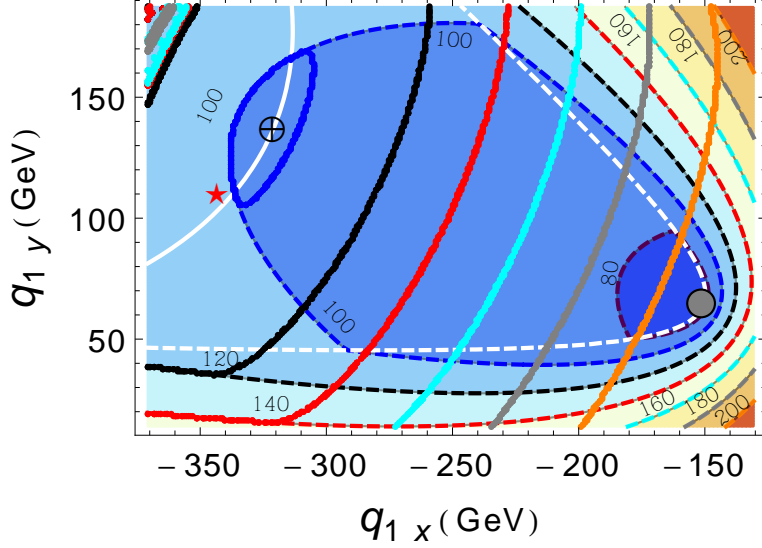


FIG. 2: The effect of the heavy resonance mass-shell constraint is demonstrated using the mass variables M_{T_2} and M_{2Cons} considering one antler event in the invisible momentum component space. The region represented by the color gradient is the maximum among two transverse masses coming from two decay chains. Corresponding contours are shown with dashed lines. Following Eq. 1, the minimization of this quantity, the M_{T_2} , is represented by the filled circle ●. In the same plot, the solid lines (of same colors) are delineating the corresponding contours for the (1 + 3)-dimensional new variable with heavy resonance mass-shell constraint as in Eq. 9. Note that only the contour lines are shown in this case, not the color gradient as in the transverse mass case. The minimum of these solid contours is represented by the M_{2Cons} , displayed by circle plus ⊕ in the same figure. The G mass-shell constraint restricts the invisible momenta, making the region shrink, as depicted by the dashed and solid lines. The white dashed (solid) line represents the equality of transverse-mass (mass) of parents and this equality line is also moving towards higher values because of the constraint. The red star ★ is the position of true transverse momenta of invisible particle. The mass spectrum we choose is $(m_G, m_P, m_\chi) = (1000.0, 200.0, 100.0)$ in GeV and the trial invisible particle mass \tilde{m}_χ we took for this plot is 10.0 GeV

To write in a compact form,

$$M_{2Cons}^{max}(\tilde{m}_\chi) \begin{cases} = M_2^{max}(\tilde{m}_\chi) = m_P, & \text{if } \tilde{m}_\chi = m_\chi \\ > M_2^{max}(\tilde{m}_\chi), & \text{if } \tilde{m}_\chi \neq m_\chi. \end{cases} \quad (10)$$

While this point is further discussed in the following section as a means of measuring the

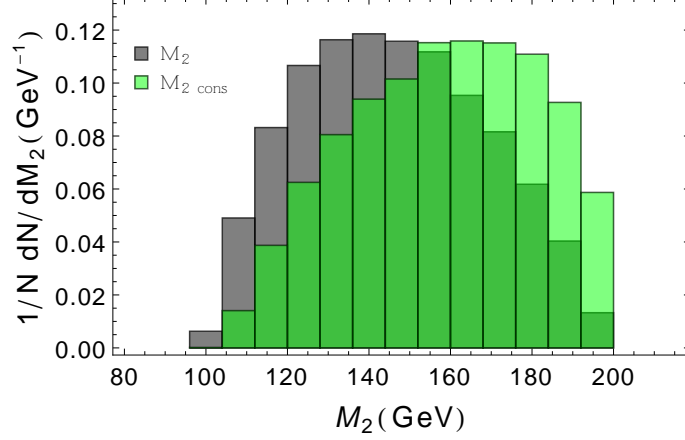


FIG. 3: Normalized distributions of the mass variables are delineated using a toy model of antler topology with parents mass at 200 GeV. Both the M_2 (dark) and $M_{2\text{cons}}$ (green) distributions, considering the invisible particle mass at its true value (100 GeV), produce the end point at the correct parent mass. However, the heavy resonance constraint gives $M_{2\text{cons}}$ a higher value, resulting a larger number of events at the end point.

unknown masses, here we illustrate it with one example distribution for the aforementioned M_2 variables, considering a toy process with the antler topology as shown in Fig. 1. For demonstration purposes, we choose a mass spectrum with $\{m_G, m_P, m_\chi\} = \{1000, 200, 100\}$ in GeV, which is a relatively difficult region for the kinematic cusp method [49, 50] known as the “large mass gap” region, where the cusp may not be very sharp, leading to large errors in the mass determination. The $M_{2\text{Cons}}$ variable can be effective for mass determination both in the large mass gap region as well as in other regions of phase space. In Fig. 3, we have compared the normalized distributions for M_2 and $M_{2\text{Cons}}$ at the true mass of the invisible particle. Both the constrained (green histogram) and unconstrained (dark histogram) distributions share the same end point precisely at the parent mass, as argued earlier. However, from the distribution, one should also note the movement of the events towards the higher value under the heavy resonance constraint and, thus, expect a larger number of events at the end point.

III. MASS MEASUREMENTS WITH KINK

Kink in mass measurement techniques is a widely acclaimed feature, first shown in the context of the M_{T2} variable. Let us continue from the brief discussion below Eq. 1 where the distribution maximum $M_{T2}^{max}(\tilde{m}_\chi)$ is observed to offer a useful relation correlating the parent mass with the trial value of unknown invisible mass \tilde{m}_χ . It is shown [26, 27] that simultaneously both parent mass m_P and daughter mass m_χ can be determined by identifying a kink (continuous but not differentiable) in this correlation curve, where the true mass point resides. It is worthy of attention that the $M_{T2}^{max}(\tilde{m}_\chi)$ has two different functional forms before and after this kink, and they share the same value at the true mass point. This behavior stems from the fact that the visible system invariant mass of any (or both) decay chain(s) have to have a range of values; hence, there should be at least two visible particles per decay chain. Consequently, experimentally simpler single-step decay chain topology is deprived of such advantage. The above feature was shown where the system does not have any recoil from initial state radiation (ISR) or upstream transverse momenta (UTM). But the presence of ISR is inevitable during the production at any hadron collider. It is subsequently revealed [28, 29, 31] that kink can also arise from topology having a single-step decay chain on both sides, but there should be recoil to the system which may come from ISR or UTM. Both scenarios can naturally arise in subsystem context from a longer decay chain. However, sizable kink resolution only comes from the events with very high recoil P_T , essentially with very low statistics.

In the last section, we define the constrained variable M_{2Cons} using the heavy resonance on-shell constraint in the minimization of M_2 . Analogous to the previous discussion,⁷ the maximum of this variable M_{2Cons}^{max} also exhibits different dependence at either side from true mass, as a function of trial invisible particle mass \tilde{m}_χ . Following the Eq. 10, one can obtain the kink structure exactly at the true mass. However, the source for the appearance of this kink is attributed to the heavy resonance mass-shell constraint in the minimization.⁸

⁷ At this point, we would like to make it clear that the effect of ISR/UTM is not considered in this present analysis. This study shows a new kink solution due to the kinematic constraint coming from on-shell mass resonance in antler events. If one consider such events associated with ISR, that may marginally contribute strengthening the case over already strong kink solution as demonstrated.

⁸ One can argue that the heavy resonance constraint works in the same spirit of ‘relative’ constraint as defined in M_2 class of variables [42]. In fact, in a non-antler scenario the M_2 variables under usual relative

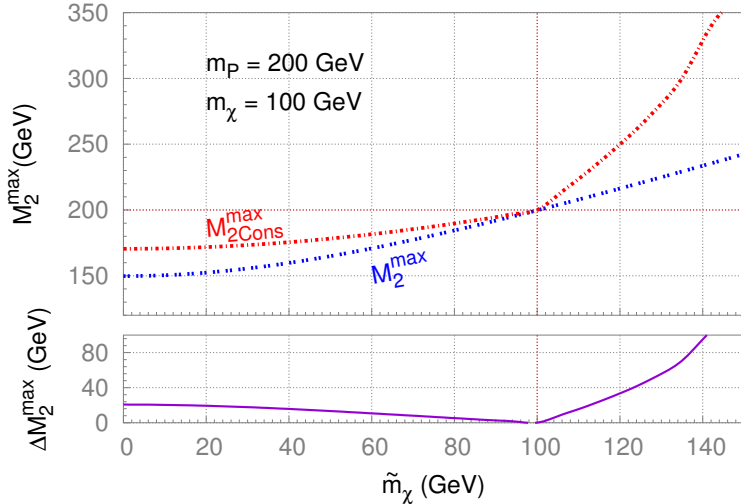


FIG. 4: Upper plot depicts the behavior of the upper end points for both the constrained $M_{2Cons}^{max}(\tilde{m}_\chi)$ and unconstrained $M_2^{max}(\tilde{m}_\chi)$ variables with respect to the trial invisible particle mass \tilde{m}_χ . The blue dashed line portrays $M_2^{max}(\tilde{m}_\chi)$, the red dashed line $M_{2Cons}^{max}(\tilde{m}_\chi)$ and the red thin dotted lines intersect at the value of true masses. This plot clearly illustrates that because of the on-shell constraint, M_{2Cons} attains a larger value, even bigger than the corresponding M_2^{max} once \tilde{m}_χ is different from the true mass m_χ . The most compelling observation about this plot is the appearance of a kink exactly at the true mass point for $M_{2Cons}^{max}(m_\chi)$, which can be used solely for measuring both m_P and m_χ simultaneously. The lower plot describes the difference $M_{2Cons}^{max}(\tilde{m}_\chi) - M_2^{max}(\tilde{m}_\chi)$ with respect to the trial invisible particle mass \tilde{m}_χ . As expected, the difference between both the end points is zero at the true invisible particle mass.

Although there is no analytic formula in support of the above empirical observation, we verified it by checking the slope numerically before and after the true mass point. The presence of this kink is also authenticated by various mass spectrums. Also note that unlike $M_2^{max}(\tilde{m}_\chi)$, the constrained variable $M_{2Cons}^{max}(\tilde{m}_\chi)$ cannot increase forever with the increase of the trial invisible particle mass \tilde{m}_χ , owing to the additional heavy resonance mass-shell constraint. M_{2Cons}^{max} can maximally reach up to half of the resonant mass and after that it would be unphysical. We have not studied the effects of ISR or UTM on this kink solution,

constraints extend/shift their distribution end-point value over and above the end point where this relative constraint is absent. Similar to our case, this can happen when trial mass deviates from true the invisible particle mass. Hence, one expects formation or consolidation of similar kink structure.

but one expects that the presence of those extra transverse momenta will sharpen the kink structure, leaving these realistic studies for future work.

To demonstrate this behavior in a more quantitative sense, we once again consider the toy process with the antler topology with the aforementioned mass spectrum. The top plot of Fig. 4 depicts the dependence of both $M_2^{max}(\tilde{m}_\chi)$ as well as the constrained $M_{2Cons}^{max}(\tilde{m}_\chi)$ with respect to the trial invisible particle mass \tilde{m}_χ . The red thin dotted lines showing true mass lines intersect at the true mass point, $\{m_\chi, m_P\} = \{100, 200\}$ in GeV. This plot clearly illustrates that because of the on-shell constraint, M_{2Cons} attains a larger value, even bigger than the corresponding M_2^{max} once \tilde{m}_χ is different from the true mass m_χ . However, both of these maximum quantities attain the same value precisely at the true mass. The most compelling observation about this plot is the appearance of a kink exactly at this point for $M_{2Cons}^{max}(\tilde{m}_\chi)$, which can be used for measuring both masses m_P and m_χ simultaneously. The bottom plot describes the variation of difference between two maximums *i.e.* $M_{2Cons}^{max}(\tilde{m}_\chi) - M_2^{max}(\tilde{m}_\chi)$ with respect to the trial invisible particle mass \tilde{m}_χ . As expected, this difference between both the end points should ideally be zero at the true invisible particle mass.

IV. MORE ASPECTS OF KINK MEASUREMENT

One of the significant challenges with most of the mass variables is the detection of the distribution end point, which can reach to the theoretical maximum only after using a large amount of data with significant statistics. The problem comes from the fact that negligible amount of events typically contribute towards the distribution end point. M_{2Cons} is also not an exception, forming a tail in the distribution towards its maximum value.⁹

This feature is clarified in Fig. 5 where the density of events is displayed as a percentage of total data contributing to the M_2 distributions. As a function of the trial invisible mass \tilde{m}_χ , the left plot shows the reference density for the M_2 distribution which can reach up to a maximum, above which there are no events and it remains white. For the same data set, the right plot shows the density of events for the constrained variable M_{2Cons} . The color coding represents the percentage of events per 2 GeV bin in M_2 . These upper end points are equivalent to the maximum curve in Fig. 4, in the last section. Compared to

⁹ On the contrary, at the true invisible mass, M_{2Cons} produces a sharper end point as demonstrated in figure 3.

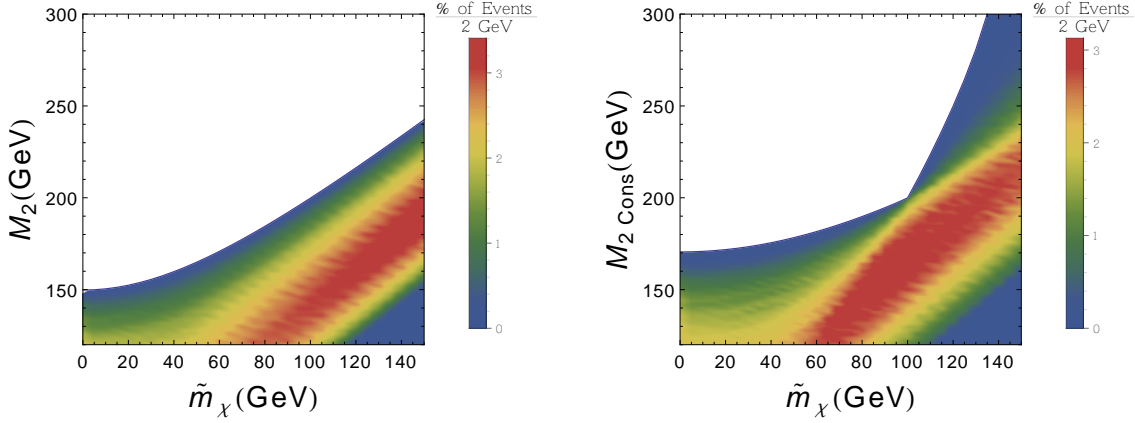


FIG. 5: Density of events as a percentage of total data contributing to M_2 distributions as a function of the trial invisible mass \tilde{m}_χ . On the left, the reference figure is shown for the M_2 variable which does not include heavy resonance constraint. The similar figure on the right is for the constrained variable M_{2Cons} , where constraint refers to the G mass-shell constraint. The color coding represents the percentage of events per 2 GeV bin in M_2 . Since this distribution reaches a maximum for every trial value of \tilde{m}_χ , above which there are no events, this disallowed range kept as white. This upper end point in each plot represents the maximum curve shown in Fig. 4, last section. The presence of the kink can be clearly seen from the figure, and it is solely because of the on-shell heavy resonance constraint. But the reconstruction of the kink can be challenging due to the much smaller number of events at the endpoint, specifically when away from the kink. Also, it is interesting to note the changes in event density due to the application of an additional constraint. Evidently, a significant number of events shifted towards the end point at the true mass, as can be observed in the figure.

the left figure, M_{2Cons} developed a clear kink solely because of the on-shell constraint of the heavy resonance. One notices that a tiny fraction of events is actually contributing at the end point, specifically when away from the kink position. Also, it is interesting to note the changes in event density due to the additional constraint. At the true mass (kink), a significant number of events shifted towards the end point, as is also observed in Fig. 3. This demonstration is also generated considering the toy process with the antler topology with the aforementioned mass spectrum $\{m_G, m_P, m_\chi\} = \{1000, 200, 100\}$ in GeV.

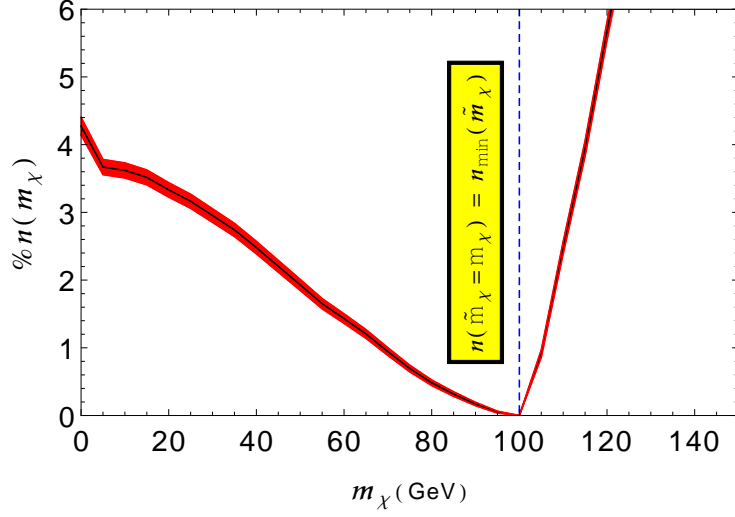


FIG. 6: The effectiveness of the variable $n(\tilde{m}_\chi)$ as defined in Eq. 11 is in identifying the minimum and thus measuring the true mass of the invisible daughter. The function as a percentage of the event fraction clearly shows a sharp minimum at $\tilde{m}_\chi = m_\chi$. So by identifying the minimum of $n(\tilde{m}_\chi)$, one can measure the invisible particle mass accurately. The red band shows the error accounting only for the statistical uncertainty.

We pointed out and discussed the difficulty with determining the end points, which is in no way a shortcoming for this variable only. Fortunately, in this present case, the ability to simultaneously identify both M_2 and M_{2Cons} provides a solution for effectively pointing out the kink using all the events, not just relying on the events at the maximum.

We have already discussed in Sec. II that the additional constraint pushes the M_{2Cons} towards the higher value compared to M_2 , such that, as long as the trial invisible mass \tilde{m}_χ is unequal to the true mass m_χ , there can be enough events generating a larger M_{2Cons} than M_2^{max} . Moreover, it is clear from Eq. 10 that the M_{2Cons}^{max} coincides with M_2^{max} at the true invisible mass. This enables us to define a dimensionless variable pointing out the position of kink, in a way that was originally proposed in [32]. For a given \tilde{m}_χ , one counts all the events having M_{2Cons} value larger than the corresponding M_2^{max} to get the fraction,

$$n(\tilde{m}_\chi) = \frac{1}{N} \mathcal{N}(\tilde{m}_\chi) = \frac{1}{N} \sum_{i=1}^N \mathcal{H}_i(M_{2Cons}(\tilde{m}_\chi) - M_2^{max}(\tilde{m}_\chi)). \quad (11)$$

Here i is the event index with total number N . $\mathcal{N}(\tilde{m}_\chi)$ is the number of events in which

$M_{2Cons}(\tilde{m}_\chi) > M_2^{max}(\tilde{m}_\chi)$ for any given \tilde{m}_χ , satisfied by the Heaviside step function,

$$\mathcal{H}_i(y) = \begin{cases} 0, & \text{if } y \leq 0 \\ 1, & \text{if } y > 0. \end{cases} \quad (12)$$

It is easy to follow from Eq. 10 that the quantity $n(\tilde{m}_\chi)$ should ideally be zero at the true mass m_χ since both M_{2Cons} and M_2 share the same maximum value at that point. However, on both sides away from this point, substantial events contribute above the M_2^{max} ; hence, $n(\tilde{m}_\chi)$ poses a sharp minimum at the true mass point. Considering other realistic effects, such as backgrounds, mass width, and experimental errors, can lift the minimum from zero. These effects are not considered in this present analysis. However, it is safe to assume that the position of the functional minimum can be correctly identified to get the true invisible mass. The advantage of using $n(\tilde{m}_\chi)$ is that it does not rely on some isolated event at the end point but rather it relies on a significant number of events distributed on a band in a two-dimensional plane between M_2^{max} and M_{2Cons}^{max} which contribute to establish this minimum.

In our example, theoretical prediction of the function $n(\tilde{m}_\chi)$ (as a fraction of total events) is shown in Fig. 6. The red band is the error accounting only for the statistical uncertainty. One can clearly identify the minimum and justify the relation

$$n(\tilde{m}_\chi = m_\chi) \equiv n_{min}(\tilde{m}_\chi) \quad (13)$$

to measure the invisible particle mass accurately. Hence, it is straightforward to measure both the parent and daughter masses simultaneously.

V. RECONSTRUCTION CAPABILITY OF EVENTS

In this section, we are inclined to explore the event reconstruction capability coming from the constrained mass variable M_{2Cons} , typically once the invisible particle mass is determined, as in last section. Event reconstruction is extremely important in the case of spin, polarization and the coupling determination of new physics as well as SM processes with the Higgs and top. However, it is almost impossible to determine them exactly for a scenario involving multiple invisible particles in a hadron collider, especially for a topology with a short decay chain. Attempts have been made to reconstruct events using the transverse

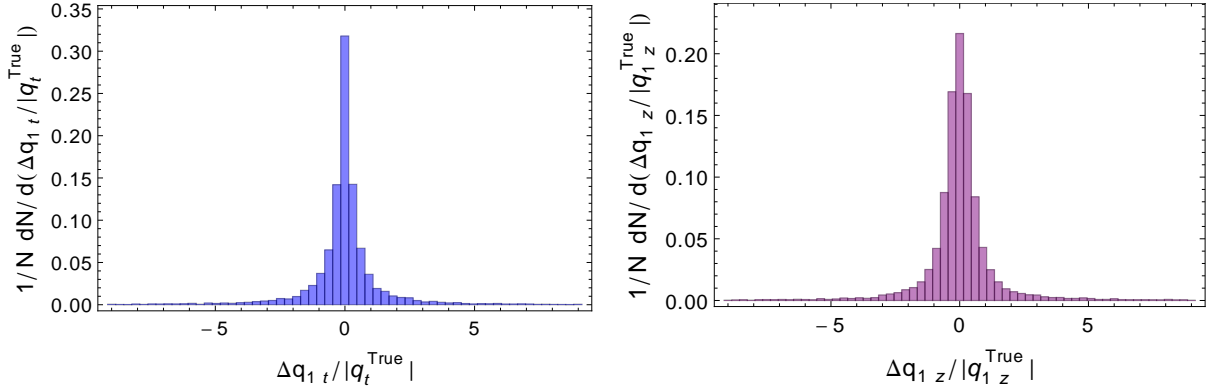


FIG. 7: Capability of reconstructing missing daughters momenta is demonstrated using constrained variable. Left figure is displaying a normalised distribution of $\frac{\Delta q_{1t}}{|q_{1t}^{True}|}$ with $\Delta q_{1t} = q_{1t}^{reco} - q_{1t}^{True}$, hence parameterize the deviation from true momenta for the transverse part, With "t" either x or y-component of momenta. This reconstruction of momenta is done from the minimisation of the M_{2Cons} with the true mass of the invisible particle as input. The reconstructed invisible momenta is unique and very well correlated with true momenta as the distribution of $\frac{\Delta q_{1t}}{|q_{1t}^{True}|}$ has a sharp peak at zero. In a process where the invisible particle mass is unknown, $n(m_\chi)$ can be used for invisible particle mass determination and then event reconstruction using M_{2Cons} . Similarly, right figure displays a normalised distribution of $\frac{\Delta q_{1z}}{|q_{1z}^{True}|}$ with $\Delta q_{1z} = q_{1z}^{reco} - q_{1z}^{True}$ for more troublesome longitudinal momentum. Once again, q_{1z} reconstruction is unique and well correlated with true longitudinal momenta of invisible particle.

mass variable M_{T2} [59–61] known as the M_{T2} -assisted on-shell (MAOS) method in which the transverse momenta of the invisible particle are determined from the minimization of M_{T2} , and the longitudinal components are determined by solving mass-shell the constraints of parent and daughter. In Ref. [47, 48], it is shown that \hat{s}_{min} and its constrained sisters \hat{s}_{min}^{cons} and \hat{s}_{max}^{cons} , can also be used for event reconstruction especially in antler topology, where constraints refer to missing transverse momenta and available mass-shell constraints in an event. The reconstructed momenta of the invisible particles are derived at the extremum of \hat{s} and the constrained \hat{s} variables.

In this section we reconstruct all components of the invisible particle momenta from minimization of the $(1 + 3)$ -dimensional variable M_{2Cons} with the true mass of the invisible particle as input. The capability of reconstructing the missing daughters momenta is demonstrated in Fig. 7 using this constrained variable. The left plot displays a normalized

distribution of the deviation (or error) in this reconstructed quantity from that of the true value, in the case of transverse part of the invisible momenta. This deviation is parametrized using a ratio defined as

$$\frac{q_{1t}^{reco} - q_{1t}^{True}}{|q_{1t}^{True}|}, \quad (14)$$

where the subscript "t" refers to the transverse (x or y) component of momenta. The reconstructed invisible momenta are proved to be unique and very well correlated with the true momenta, as the observed distribution has a sharp peak at its true value (*i.e.* zero deviation). Similarly, the right figure displays a normalized distribution of the corresponding variable for longitudinal momentum, and once again one gets a unique reconstruction well correlated with the true longitudinal momenta of the invisible particle. In a process where the invisible particle mass is unknown, $n(m_\chi)$ can be used for invisible particle mass determination, and then events can be reconstructed using M_{2Cons} .

VI. SUMMARY AND CONCLUSIONS

Looking forward to another breakthrough in the second phase of its journey, the LHC is discovering credible hints for new physics. Many of the popular BSM models are extended with massive exotic dark matter particles. As a result, common signatures, coming from such models at a high-energy collider, typically are detectable SM particles along with a pair of invisible particles. They are too complex to measure all the unknown masses or to fully reconstruct those events at the large hadron collider.

In this paper, we study one such class of events produced through antler topology. They are common in SM Higgs and several BSM scenarios, where the heavy resonance is produced before semi-invisible decay into visible decay products together with invisibles which can either be SM neutrinos or some exotic dark matter particles. Our objective is to determine all the unknown masses, including the dark matter particles produced from the heavy resonance. We consider a new constrained variable M_{2Cons} extending the (1 + 3)-dimensional mass variable M_2 , by implementing additional heavy grandparent mass-shell constraint in the minimization.

This new variable M_{2Cons} contains several interesting features. We demonstrate how this variable acquires an event wise higher value owing to this constraint. In particular, we show how this variable moves closer to the unknown parent mass. In addition, the calculated

invisible momenta at this minimum can provide a close estimate of the true momenta of the invisible particles for such events. Both these characteristic features are highlighted and exploited further to sharpen the measurements.

Another striking feature comes out once we analyze the distribution maxima of this new variable $M_{2Cons}^{max}(\tilde{m}_\chi)$ as a function of the trial values of yet unknown dark matter particle mass. This is constructed in an analogy with the popular study of $M_{T2}^{max}(\tilde{m}_\chi)$, which gives a useful correlation curve relating the parents mass with the invisible particle mass. But now, under mass-shell constraint, $M_{2Cons}^{max}(\tilde{m}_\chi)$ develops a new kink solution over the correlation curve exactly at the value where this trial mass coincides with the true mass. Hence, this opened another new avenue that produces a kink feature to measure both masses simultaneously.

To handle the sparseness of events towards the distribution end point, we analyze with an experimentally feasible observable $n(\tilde{m}_\chi)$ by utilizing both constrained and unconstrained variables. This observable does not rely on isolated events at the end point, but instead uses a significant amount of available data to pinpoint the unknown invisible particle mass from the sharp minimum.

Our method provides a complementary procedure to earlier antler studies and is applicable to any mass region. We demonstrate our analysis in the large mass gap region, considered as a difficult region for the kinematic cusp method. In this region, the cusps of many variables are not very sharp, which makes the mass determination more prone to error. But the present method can be used safely for better accuracy. We also investigate the event reconstruction capability of M_{2Cons} , and we reconstruct the unknown invisible particle momenta at the constrained minimization. The reconstructed momenta are found to be unique and well correlated with the true invisible momenta.

Acknowledgments

This work was funded by the Physical Research Laboratory (PRL), Department of Space (DoS), India. PK also gratefully acknowledges IACS and IISER Kolkata for hospitality.

- [1] Serguei Chatrchyan et al. Observation of a new boson at a mass of 125 GeV with the CMS experiment at the LHC. *Phys.Lett.*, B716:30–61, 2012.
- [2] Georges Aad et al. Observation of a new particle in the search for the Standard Model Higgs boson with the ATLAS detector at the LHC. *Phys.Lett.*, B716:1–29, 2012.
- [3] Kaustubh Agashe, Doojin Kim, Manuel Toharia, and Devin G.E. Walker. Distinguishing Dark Matter Stabilization Symmetries Using Multiple Kinematic Edges and Cusps. *Phys.Rev.*, D82:015007, 2010.
- [4] Kaustubh Agashe, Doojin Kim, Devin G.E. Walker, and Lijun Zhu. Using M_{T2} to Distinguish Dark Matter Stabilization Symmetries. *Phys.Rev.*, D84:055020, 2011.
- [5] Won Sang Cho, Doojin Kim, Konstantin T. Matchev, and Myeonghun Park. Cracking the dark matter code at the LHC. *Phys.Rev.Lett.*, 112:211801, 2014.
- [6] Gian Francesco Giudice, Ben Gripaios, and Rakhi Mahbubani. Counting dark matter particles in LHC events. *Phys.Rev.*, D85:075019, 2012.
- [7] Kaustubh Agashe, Roberto Franceschini, Doojin Kim, and Kyle Wardlow. Using Energy Peaks to Count Dark Matter Particles in Decays. *Phys. Dark Univ.*, 2:72–82, 2013.
- [8] Alan J. Barr and Christopher G. Lester. A Review of the Mass Measurement Techniques proposed for the Large Hadron Collider. *J.Phys.*, G37:123001, 2010.
- [9] A.J. Barr, T.J. Khoo, P. Konar, K. Kong, C.G. Lester, et al. Guide to transverse projections and mass-constraining variables. *Phys.Rev.*, D84:095031, 2011.
- [10] I. Hinchliffe, F.E. Paige, M.D. Shapiro, J. Soderqvist, and W. Yao. Precision SUSY measurements at CERN LHC. *Phys.Rev.*, D55:5520–5540, 1997.
- [11] B.K. Gjelsten, D.J. Miller, and P. Osland. Measurement of SUSY masses via cascade decays for SPS 1a. *JHEP*, 0412:003, 2004.
- [12] B.C. Allanach, C.G. Lester, Michael Andrew Parker, and B.R. Webber. Measuring sparticle masses in nonuniversal string inspired models at the LHC. *JHEP*, 0009:004, 2000.

- [13] Mihoko M. Nojiri, Daisuke Toya, and Tomio Kobayashi. Lepton energy asymmetry and precision SUSY study at hadron colliders. *Phys.Rev.*, D62:075009, 2000.
- [14] B.K. Gjelsten, D.J. Miller, and P. Osland. Measurement of the gluino mass via cascade decays for SPS 1a. *JHEP*, 0506:015, 2005.
- [15] Michael Burns, Konstantin T. Matchev, and Myeonghun Park. Using kinematic boundary lines for particle mass measurements and disambiguation in SUSY-like events with missing energy. *JHEP*, 0905:094, 2009.
- [16] Konstantin T. Matchev, Filip Moortgat, Luc Pape, and Myeonghun Park. Precise reconstruction of sparticle masses without ambiguities. *JHEP*, 0908:104, 2009.
- [17] M. M. Nojiri, G. Polesello, and D. R. Tovey. Proposal for a new reconstruction technique for SUSY processes at the LHC. In *Physics at TeV colliders. Proceedings, Workshop, Les Houches, France, May 26-June 3, 2003*.
- [18] K. Kawagoe, M.M. Nojiri, and G. Polesello. A New SUSY mass reconstruction method at the CERN LHC. *Phys.Rev.*, D71:035008, 2005.
- [19] Hsin-Chia Cheng, John F. Gunion, Zhenyu Han, Guido Marandella, and Bob McElrath. Mass determination in SUSY-like events with missing energy. *JHEP*, 0712:076, 2007.
- [20] Mihoko M. Nojiri and Michihisa Takeuchi. Study of the top reconstruction in top-partner events at the LHC. *JHEP*, 0810:025, 2008.
- [21] Hsin-Chia Cheng, Dalit Engelhardt, John F. Gunion, Zhenyu Han, and Bob McElrath. Accurate Mass Determinations in Decay Chains with Missing Energy. *Phys.Rev.Lett.*, 100:252001, 2008.
- [22] C.G. Lester and D.J. Summers. Measuring masses of semiinvisibly decaying particles pair produced at hadron colliders. *Phys.Lett.*, B463:99–103, 1999.
- [23] Alan Barr, Christopher Lester, and P. Stephens. $m(T2)$: The Truth behind the glamour. *J.Phys.*, G29:2343–2363, 2003.
- [24] Patrick Meade and Matthew Reece. Top partners at the LHC: Spin and mass measurement. *Phys.Rev.*, D74:015010, 2006.
- [25] Christopher Lester and Alan Barr. MTGEN: Mass scale measurements in pair-production at colliders. *JHEP*, 0712:102, 2007.
- [26] Won Sang Cho, Kiwoon Choi, Yeong Gyun Kim, and Chan Beom Park. Gluino Stransverse Mass. *Phys.Rev.Lett.*, 100:171801, 2008.

- [27] Won Sang Cho, Kiwoon Choi, Yeong Gyun Kim, and Chan Beom Park. Measuring superparticle masses at hadron collider using the transverse mass kink. *JHEP*, 0802:035, 2008.
- [28] Alan J. Barr, Ben Gripaios, and Christopher G. Lester. Weighing Wimps with Kinks at Colliders: Invisible Particle Mass Measurements from Endpoints. *JHEP*, 0802:014, 2008.
- [29] Ben Gripaios. Transverse observables and mass determination at hadron colliders. *JHEP*, 0802:053, 2008.
- [30] Mihoko M. Nojiri, Yasuhiro Shimizu, Shogo Okada, and Kiyotomo Kawagoe. Inclusive transverse mass analysis for squark and gluino mass determination. *JHEP*, 0806:035, 2008.
- [31] Michael Burns, Kyoungchul Kong, Konstantin T. Matchev, and Myeonghun Park. Using Subsystem MT_2 for Complete Mass Determinations in Decay Chains with Missing Energy at Hadron Colliders. *JHEP*, 0903:143, 2009.
- [32] Partha Konar, Kyoungchul Kong, Konstantin T. Matchev, and Myeonghun Park. Superpartner Mass Measurement Technique using 1D Orthogonal Decompositions of the Cambridge Transverse Mass Variable M_{T2} . *Phys.Rev.Lett.*, 105:051802, 2010.
- [33] Won Sang Cho, Jihn E. Kim, and Ji-Hun Kim. Amplification of endpoint structure for new particle mass measurement at the LHC. *Phys.Rev.*, D81:095010, 2010.
- [34] Won Sang Cho, William Klemm, and Mihoko M. Nojiri. Mass measurement in boosted decay systems at hadron colliders. *Phys.Rev.*, D84:035018, 2011.
- [35] Alan J. Barr, Ben Gripaios, and Christopher G. Lester. Transverse masses and kinematic constraints: from the boundary to the crease. *JHEP*, 0911:096, 2009.
- [36] Partha Konar, Kyoungchul Kong, Konstantin T. Matchev, and Myeonghun Park. Dark Matter Particle Spectroscopy at the LHC: Generalizing $M(T_2)$ to Asymmetric Event Topologies. *JHEP*, 1004:086, 2010.
- [37] Daniel R. Tovey. On measuring the masses of pair-produced semi-invisibly decaying particles at hadron colliders. *JHEP*, 0804:034, 2008.
- [38] Giacomo Polesello and Daniel R. Tovey. Supersymmetric particle mass measurement with the boost-corrected contranverse mass. *JHEP*, 1003:030, 2010.
- [39] Mario Serna. A Short comparison between $m(T_2)$ and $m(CT)$. *JHEP*, 0806:004, 2008.
- [40] Konstantin T. Matchev and Myeonghun Park. A General method for determining the masses of semi-invisibly decaying particles at hadron colliders. *Phys.Rev.Lett.*, 107:061801, 2011.
- [41] Rakhi Mahbubani, Konstantin T. Matchev, and Myeonghun Park. Re-interpreting the

- Oxbridge stransverse mass variable MT_2 in general cases. *JHEP*, 1303:134, 2013.
- [42] Won Sang Cho, James S. Gainer, Doojin Kim, Konstantin T. Matchev, Filip Moortgat, et al. On-shell constrained M_2 variables with applications to mass measurements and topology disambiguation. *JHEP*, 1408:070, 2014.
- [43] D.R. Tovey. Measuring the SUSY mass scale at the LHC. *Phys.Lett.*, B498:1–10, 2001.
- [44] Jay Hubisz, Joseph Lykken, Maurizio Pierini, and Maria Spiropulu. Missing energy look-alikes with 100 pb^{-1} at the LHC. *Phys.Rev.*, D78:075008, 2008.
- [45] Partha Konar, Kyoungchul Kong, and Konstantin T. Matchev. $\sqrt{\hat{s}_{min}}$: A Global inclusive variable for determining the mass scale of new physics in events with missing energy at hadron colliders. *JHEP*, 0903:085, 2009.
- [46] Partha Konar, Kyoungchul Kong, Konstantin T. Matchev, and Myeonghun Park. RECO level \sqrt{s}_{min} and subsystem \sqrt{s}_{min} : Improved global inclusive variables for measuring the new physics mass scale in \cancel{E}_T events at hadron colliders. *JHEP*, 1106:041, 2011.
- [47] Abhaya Kumar Swain and Partha Konar. Constrained $\sqrt{\hat{S}_{min}}$ and reconstructing with semi-invisible production at hadron colliders. *JHEP*, 1503:142, 2015.
- [48] Abhaya Kumar Swain and Partha Konar. Mass determination and event reconstruction at Large Hadron Collider. *Springer Proc. Phys.*, 174:599–603, 2016.
- [49] Tao Han, Ian-Woo Kim, and Jeonghyeon Song. Kinematic Cusps: Determining the Missing Particle Mass at Colliders. *Phys.Lett.*, B693:575–579, 2010.
- [50] Tao Han, Ian-Woo Kim, and Jeonghyeon Song. Kinematic Cusps With Two Missing Particles I: Antler Decay Topology. *Phys.Rev.*, D87(3):035003, 2013.
- [51] Tao Han, Ian-Woo Kim, and Jeonghyeon Song. Kinematic Cusps with Two Missing Particles II: Cascade Decay Topology. *Phys.Rev.*, D87(3):035004, 2013.
- [52] Neil D. Christensen, Tao Han, Zhuoni Qian, Josh Sayre, Jeonghyeon Song, et al. Determining the Dark Matter Particle Mass through Antler Topology Processes at Lepton Colliders. *Phys.Rev.*, D90:114029, 2014.
- [53] Abdelhak Djouadi. The Anatomy of electro-weak symmetry breaking. II. The Higgs bosons in the minimal supersymmetric model. *Phys.Rept.*, 459:1–241, 2008.
- [54] Matthew Baumgart, Thomas Hartman, Can Kilic, and Lian-Tao Wang. Discovery and measurement of sleptons, binos, and winos with a Z-prime. *JHEP*, 0711:084, 2007.
- [55] Mirjam Cvetič and P. Langacker. Z-prime physics and supersymmetry. *Adv.Ser.Direct.High*

- Energy Phys.*, 21:325–350, 2010.
- [56] Hsin-Chia Cheng, Jonathan L. Feng, and Konstantin T. Matchev. Kaluza-Klein dark matter. *Phys.Rev.Lett.*, 89:211301, 2002.
- [57] AseshKrishna Datta, Kyoungchul Kong, and Konstantin T. Matchev. Discrimination of supersymmetry and universal extra dimensions at hadron colliders. *Phys.Rev.*, D72:096006, 2005.
- [58] Gulab Bambhaniya, Joydeep Chakraborty, Srubabati Goswami, and Partha Konar. Generation of neutrino mass from new physics at TeV scale and multilepton signatures at the LHC. *Phys.Rev.*, D88(7):075006, 2013.
- [59] Won Sang Cho, Kiwoon Choi, Yeong Gyun Kim, and Chan Beom Park. M(T2)-assisted on-shell reconstruction of missing momenta and its application to spin measurement at the LHC. *Phys.Rev.*, D79:031701, 2009.
- [60] Diego Guadagnoli and Chan Beom Park. M_{T2} -reconstructed invisible momenta as spin analyzers, and an application to top polarization. *JHEP*, 1401:030, 2014.
- [61] Chan Beom Park. Reconstructing the heavy resonance at hadron colliders. *Phys.Rev.*, D84:096001, 2011.